

# EVALUATION OF LED AND TUNGSTEN-HALOGEN LIGHTING FOR FECAL CONTAMINANT DETECTION

K. C. Lawrence, B. Park, G. W. Heitschmidt, W. R. Windham, C. N. Thai

**ABSTRACT.** *Lighting in imaging systems plays an important role in image quality. Recent research in detecting fecal contaminants on poultry carcasses with multispectral and/or hyperspectral imaging has relied on common quartz tungsten halogen lamps for illumination. However, as the technology is implemented in a processing plant environment, there is a need to enclose the system to protect it from the harsh environment. This can result in significant challenges in maintaining quality lighting and images due to excessive heat build-up in the system enclosure, degradation in illumination, and frequent bulb changes because of shorter bulb life. Recent advances in high-power white LEDs have provided a feasible alternative to incandescent lighting. This research compared high-power LED lighting to traditional tungsten halogen lamps for contaminant detection. Sixteen contaminant samples of duodenum, ceca, and colon feces, and ingesta were imaged at four different contaminant spot sizes with two different orientations relative to a hyperspectral imaging camera. Detection accuracies were generally better than 99% for all contaminant types and either lighting system although there was one colon sample that had a rather low accuracy, most likely due to blood in the sample. Results indicate that there was no significant difference in detecting fecal contaminants with the fecal detection algorithm that uses the ratio of images centered at 565 and 517 nm with either lighting system. The overall detection accuracies were 99.63% and 99.69% for the LED and tungsten halogen lighting systems, respectively. Thus, the advantages of longer bulb life and less heat with LED lighting make it a feasible alternative to traditional lighting, provided that the LED junction temperatures are held relatively constant.*

**Keywords.** *Quartz tungsten halogen, Light emitting diodes, Poultry, Feces, Chickens, Hyperspectral imaging, Multispectral imaging.*

**L**ighting for machine vision and hyperspectral imaging is an important component for collecting high quality images. Yet, it is often given minimal consideration in the overall design of an imaging system. Tungsten-halogen lamps with quartz reflectors are the most common source of illumination for broad spectrum applications such as multispectral and hyperspectral imaging. They are usually chosen because they have high output throughout the visible and into the near infrared region (400 to 900 nm), are readily available, and relatively inexpensive. Their disadvantages include a shorter bulb life, they are relatively inefficient, and they generate significant amounts of heat.

Recently, high power, broad-spectrum “white” Light-Emitting Diodes (LEDs) have been developed that can

potentially replace tungsten-halogen incandescent lamps for some applications where bulb life and thermal constraints are factors (Mueller-Mach et al., 2002; Steigerwald et al., 2002). White light from LEDs are typically generated in three ways. The first method is to mix three independent monochromatic LED sources of red, blue and green to create light that appears white to the human eye (Muthu et al., 2002). This technique could be used for multispectral imaging systems where monochromatic LED sources match the filters in the multispectral imaging system. However, for hyperspectral imaging systems and broadband multispectral imaging systems, this method does not provide illumination for much of the detector range. The second method uses an ultraviolet LED with a phosphors package to pump red, green, and blue light without leaking any of the original ultraviolet light. The third method utilizes a blue LED to pump one or more visible light-emitting phosphors integrated into the phosphor-converted LED (pc-LED) package. The phosphor then converts most of the blue light into red and green light. The pc-LED is also designed to leak some of the original blue light to make up all the components of white light. This method is the most common for producing white light from a LED. LEDs have long been known for their long life, low power, and low intensity, but recent advances in flip-chip technology has resulted in high-power LEDs (Mueller-Mach et al., 2002; Steigerwald et al., 2002). These high-power LEDs are long lasting (over 10,000 h) and generate significantly less heat than incandescent lamps. They can also be positioned in a multitude of configurations for targets with challenging geometries and can be strobed to increase their light intensity without damaging the device. Combining the broad-spectrum white LED with these other attributes

---

Submitted for review in December 2005 as manuscript number IET 6269; approved for publication by the Information & Electrical Technologies Division of ASABE in July 2007.

Mention of company or trade name is for description only and does not imply endorsement by the U.S. Department of Agriculture.

The authors are **Kurt C. Lawrence**, ASABE Member Engineer, Research Agricultural Engineer, **Bosoon Park**, ASABE Member Engineer, Research Agricultural Engineer, USDA, ARS, Russell Research Center, Athens, Georgia; **Gerald W. Heitschmidt**, Project Coordinator, Biological and Agricultural Engineering Department, University of Georgia, Athens, Georgia; **William R. Windham**, Research Animal Physiologist, USDA, ARS, Russell Research Center, Athens, Georgia; and **Chi N. Thai**, ASABE Member Engineer, Associate Professor, Biological and Agricultural Engineering Department, University of Georgia, Athens, Georgia. **Corresponding author:** Kurt C. Lawrence, USDA, ARS, P.O. Box 5677, Russell Research Center, Athens, GA 30604-5677; phone: 706-546-3527; fax: 706-546-3607; e-mail: kurt.lawrence@ars.usda.gov.

make LEDs attractive for multispectral and some hyperspectral imaging.

The U.S. Department of Agriculture, Agricultural Research Service (ARS) has been conducting research on fecal contaminant detection for several years (Park et al., 2002, 2004; Windham et al., 2003a; Lawrence et al., 2003a, 2003b) with both research-type hyperspectral imaging systems and real-time multispectral imaging systems. This research has shown that a ratio of a reflectance image centered at 565 nm divided by a reflectance image centered at 517 nm can discriminate fecal and ingesta contaminants from other carcass features. Tungsten-halogen lighting has been used with both systems. In the demanding poultry processing environment, where all equipment must run continually and be protected in a NEMA 4X enclosure, LED lighting has the potential to be a better alternative than traditional tungsten-halogen lighting for multispectral imaging systems. Additionally, research has also focused on the potential for a high-speed hyperspectral imaging system capable of operating at processing line speeds (Lawrence et al., 2006). Such a system may also benefit from LED lighting. Thus, since hyperspectral imaging requires a broader spectrum light than multispectral imaging and multispectral imaging can be considered a subset of hyperspectral imaging, this article reports on the use of high-power, white LEDs for illumination with hyperspectral imaging systems for poultry fecal detection. From these data with the hyperspectral imaging system, results for multispectral imaging will be inferred. Statistical analysis will be performed on the data to test the hypothesis that LED lighting will improve fecal detection accuracies when compared to quartz tungsten halogen lamps.

## MATERIALS AND METHODS

### FECAL SAMPLES

Thirty-two New York-dressed poultry carcasses were collected from a local poultry processing plant and immediately transported to the pilot-scale processing facility at Russell Research Center (Athens, Ga.) where they were immediately eviscerated with a commercial eviscerator. The viscera were then collected and the contaminants were harvested manually. Feces from the duodenum, ceca, and colon portions of the digestive tract were collected and stored in small plastic vials. Ingesta from the crop or gizzard were also harvested and stored. With some samples, frequently the colon samples, there was not enough digestive material from a single bird needed for the experiment. In these circumstances, digestive material from two or more birds was combined into one sample. No digestive material from any given bird was used in more than one sample. There were a total of 16 samples of each contaminant type used in the experiment. It is well known that the myoglobins in poultry skin on a carcass oxidize quickly and can change states over time when exposed to air (Windham et al., 2003b). Furthermore, since there is often no consistent method to discern mixed skin/feces pixel and the purpose of the experiment was to evaluate lighting systems which required the lights to equilibrate over time, the feces and ingesta were applied to a flat white Teflon cutting board instead of a chicken carcass. Four randomized rows with one contaminant-type sample replicated in four spots of varying

size per row were placed on the Teflon board. A black marker was used to draw a rectangle on the cutting board equivalent to the camera field of view to aid in the positioning of the contaminant spots. The diameters of the spot size varied from about 4 to 20 mm. Figure 1 shows a typical contaminant pattern as imaged by the hyperspectral imaging system. Note the small specks of ingesta contaminant above the second ingesta spot from the right and the ceca speck above the right-most ceca contaminant. Also particularly evident in the duodenum samples are two saturated specular reflectance areas in the bottom portion of the contaminants. Not shown in figure 1 are black lettering on white paper used to indicate the order of the contaminants and the black marker lines indicating the field of view.

### EQUIPMENT

#### *Hyperspectral Imaging System*

A previous version of the hyperspectral imaging system was described earlier in detail (Lawrence et al., 2003b; Park et al., 2002), but has been recently upgraded (Heitschmidt et al., 2004). The system consisted of a 1280 × 1040 pixel Sencicam QE CCD Camera (Cooke Corp., Auburn Hills, Mich.) attached to a Specim V10E enhanced imaging spectrograph with a 30- $\mu$ m slit width (Oulu, Finland). The fore optics consisted of a Model 426A motorized translation stage (Newport, Irvine, Calif.) and a Schneider Xenoplane 1.4/23-mm lens (Schneider Optics, Hauppauge, N.Y.). The camera was binned at 2 × 2 and 400 lines were collected per image resulting in a hypercube image with dimensions 640 (spatial x) × 400 (spatial y) × 520 (wavelengths). The camera was mounted on a test stand and positioned 25.5 cm above the Teflon cutting board as shown in figure 2. The field of view covered by a 400 line-scan images was 20.6 × 7 cm. The system was calibrated first for wavelengths and then to percent reflectance as described by Lawrence et al. (2003a) except that no geometric correction was needed with the enhanced spectrograph used in this work. A 30- × 30-cm 99% Spectralon Panel (Labsphere, Inc., North Sutton, N.H.) was used to calibrate the contaminant samples and to evaluate the relative change in light intensity over time and temperature. To maximize the signal-to-noise ratio of the

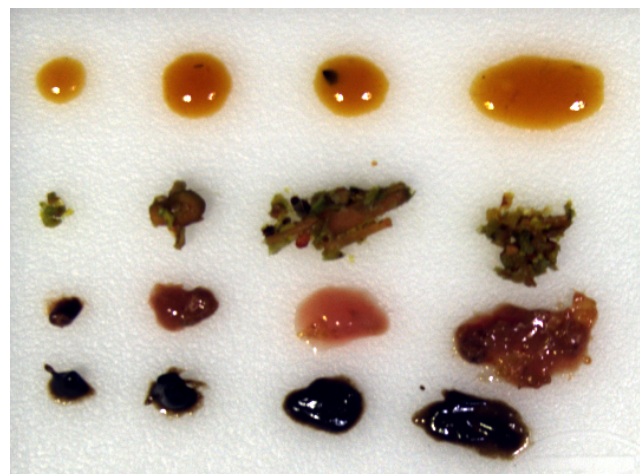


Figure 1. Color composite image of typical contaminant "spots" on Teflon cutting board taken with a hyperspectral imaging system with LED illumination. Contaminants (in rows from top) are duodenum, ingesta, colon, and ceca, with each row replicating a single contaminant sample.



Figure 2. Picture of test stand with hyperspectral imaging camera, quartz tungsten-halogen lights, and LED ring lights.

camera, the exposure time was chosen to maximize the input signal without saturating the detector. Thus, an exposure time of 13 ms was used with the LED lights and a time of 6 ms was used with the tungsten-halogen lamps.

### LEDs

High-power white LEDs in two configurations were tested. All were based on LEDs from Lumileds Lighting, LLC (San Jose, Calif.). A Luxeon six-LED Ring Light with secondary optics and an outside diameter of 74.5 mm was tested for temperature stability. Secondary optics were supplied with the emitter which produced a lambertian radiation pattern for each emitter. The nominal diameter of each emitter with optics was 21.5 mm. The ring light was mounted on an 80- × 103- × 11-mm heat sink and was powered by a recommended Xitanium17-W, 700-mA LED Electronic Drivers model LED120A0700C24F (Advance, Rosemont, Ill.). The driver had an input of 120 VAC and an output of 24VDC. Thermal grease (Wakefield Engineering, Inc., Pelham, N.H.) with a thermal conductivity of 0.735 W/m-K was used to ensure adequate heat transfer between the LED and heat sink. This first configuration was called the heat-sink LED. The second configuration was a six-LED spot light model WSP3.25-WHI from Spectrum Illumination (Muskegon, Mich.). The Spectrum Illumination light, known as a “Monster Light,” utilized the same six-LED ring light described earlier, but enclosed the light in a FDA-compliant wash-down enclosure made of Delrin and stainless steel. The monster light was powered by a BK Precision 1744 DC Power Supply operating at 24 VDC which drove a LDM Series Driver at 1.0 A. The driver was capable of operating in either continuous or strobe modes. For this study, the LED was operated in continuous mode only. The LED Monster Lights were placed 24.3 cm above the horizontal image surface and the hyperspectral camera was positioned approximately 25.5 cm from the image surface as shown in figure 2. The monster lights were positioned about 12 cm (center of light to center of lens) on either side of the camera lens, offset about 5 cm in the other direction and angled slightly towards the center of the image plane to provide uniform illumination (fig. 3).

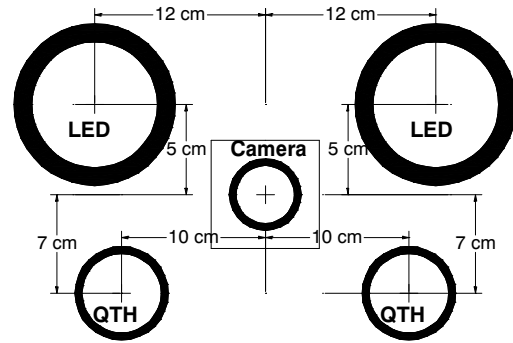


Figure 3. Top view of hyperspectral camera and two lighting system with LED and quartz-tungsten halogen (QTH) lamps. Each light was also angled towards center.

Both ambient air and LED temperatures were monitored every 30 s. with an ExTech Thermocouple Datalogging Thermometer Model EA15 (Waltham, Mass.) with a type K thermocouple.

### Quartz Tungsten Halogen Lamps

For comparison purposes, two 12-VDC, 35-W quartz tungsten-halogen (QTH) MR-16 lamps with a beam angle of 22° and frosted glass diffusers were also used. The QTH lamps were installed in Gilway lamp housings and were also powered by a BK Precision 1744 DC Power Supply. The QTH lamps were positioned 10 cm (center of light to center of lens) in front of the lens and offset by 7 cm in the other direction as shown in figure 3. The QTH lamps were about 21 cm above the imaging plane and were also angled slightly towards the center of the image plane to provide uniform illumination (fig. 2).

### Illuminance

Average light illuminance was measured periodically with a Gossen Mavolux 5032C Light Meter (Nürnberg, Germany). The light intensity was 13.23 and 5.94 klux for the quartz tungsten halogen lamps and the LEDs, respectively. Relative light intensity was measured with a hyperspectral imaging system from Photon Industries (Stennis Space Center, Miss.). The hyperspectral imaging system has a nominal spectral range from 400 to 1000 nm and was calibrated to percent reflectance as described by Lawrence et al. (2003a, 2003b).

One might argue that using both light sources after they were calibrated to percent reflectance will remove any variations caused by the light sources since measurements with both lights were calibrated with a 99% reflectance panel and dark current measurements prior to fecal contaminant measurements. Thus, regardless of the maximum detector response at a given wavelength, calibration forces that value to 99% reflectance and any lesser value is proportionately scaled down all the way to the dark current detector response. However, in practice, the light-source intensities and detector exposure times are adjusted so that the CCD detector is never saturated at the wavelengths where the response is greatest (combination of detector efficiency and light intensity). Yet those wavelengths with low detector responses will still have their reflectance response (0 to 99%) correlated with the low-response range at that wavelength, which will often be much, much less than the full-scale range of detector. Thus,

when one attempts to detect a rather dark contaminant, such as feces, on a relatively bright background (Teflon or chicken skin), then the response at many wavelengths is often very close to the noise level of the detector. Thus, errors in contaminant detection increase because of low signal-to-noise responses from the detector.

## PROCEDURE

Preliminary experiments were conducted with the heat-sink LED assembly and the QTH lamps to evaluate the temperature dependence and long-term stability of the lights. The heat-sink LED was turned on and directed towards the Spectralon panel. Images of the panel were collected with the hyperspectral imaging system every minute. One secondary optical lens was removed from the ring light and the LED junction temperature was also recorded every minute. Next a single QTH lamp was turned on and the experiment was repeated.

Since the main goal of this research was to compare the effect of two lighting systems on contaminant detection, the experiment was conducted in such a way as to use the lights under optimum conditions as determined from the preliminary experiment. Both the LED and QTH lights were allowed to warm up and stabilize prior to a measurement sequence. Furthermore, since the intensity of the LED lights are known to be temperature dependent, the LEDs were allowed to reach their equilibrium temperature of about 38°C prior to collecting images. This temperature was lower than those shown in the results because the temperature was measured on the back of the stainless plate of the Monster Light (its primary heat sink) and not at the LED junction. A measurement sequence was initiated by first collecting two calibration (99% reflectance panel) and dark current images with the LEDs. These images were later used to post-process the data and calibrate the contaminant sample images to percent reflectance. Next fecal samples were placed on the Teflon cutting board as described previously and positioned within the field of view of the imaging system. A hyperspectral image with the LEDs as a light source was then collected. To help remove the effect of spot size relative to lamp position, the Teflon cutting board was then rotated 180° and a second image was collected. LED and ambient-air temperatures were also recorded approximately every 30 s. Next, the LEDs were turned off and the QTH lamps were turned on and briefly allowed to equilibrate. Another set of calibration panel and dark current images were collected with the QTH lamps and then an image of the fecal samples was collected. As before, the Teflon board was rotated 180° and a second fecal image was collected. Once the QTH measurements were collected, the QTH lamps were turned off and the LEDs were turned back on and allowed to reach operating temperature before the process was repeated. Additionally, two calibration and dark current images were collected after every four fecal samples were imaged and finally again at the end of the experiment.

## RESULTS

### PRELIMINARY EXPERIMENTS

Figure 4 shows the spectral response of a broad-spectrum, high-power LED along with several other common light sources over the typical range of a silicon-based detector.

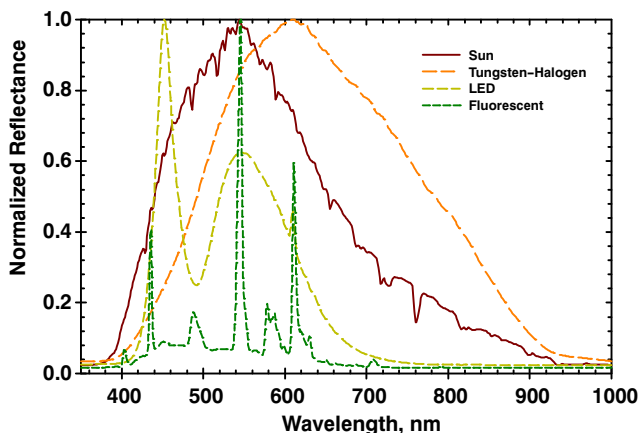


Figure 4. Typical mean spectral response of sunlight, tungsten-halogen lamps, white LEDs, and fluorescent lamps.

Data were all collected with the same hyperspectral imaging system and normalized to allow easier comparison of the spectral variations. As can be seen, the LED ring light has a reasonable spectral response from about 420 to 680 nm. Figure 5 shows the change in reflectance of the heat-sink LED versus time while figure 6 shows the temperature versus

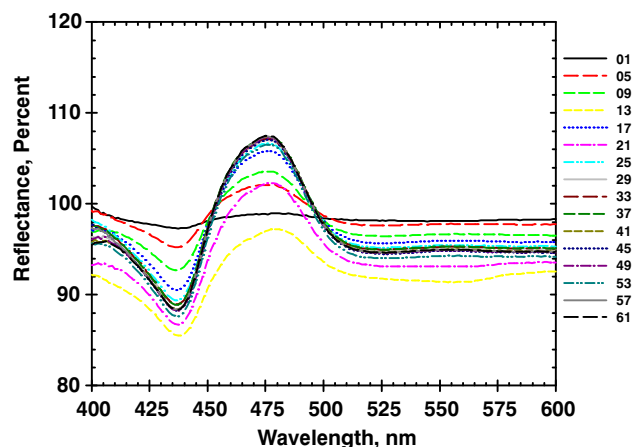


Figure 5. Mean output reflectance of Spectralon panel illuminated with heat-sink LEDs vs. time. Image at time zero was used for calibration. Legend units are in min.

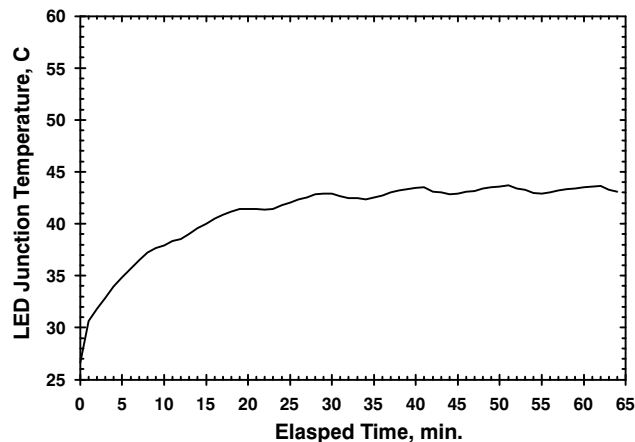
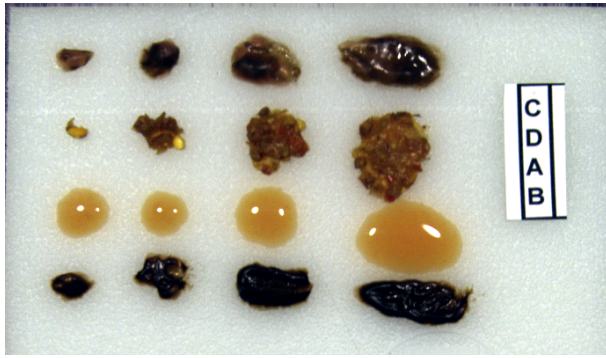
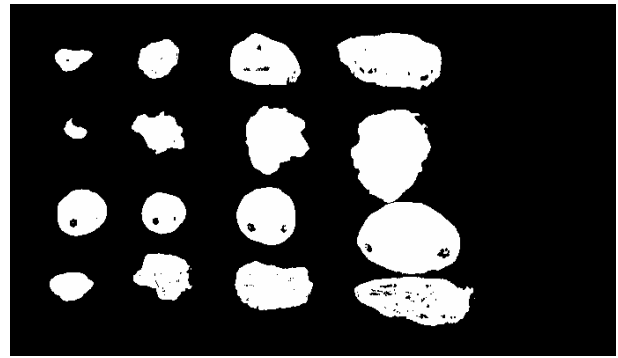


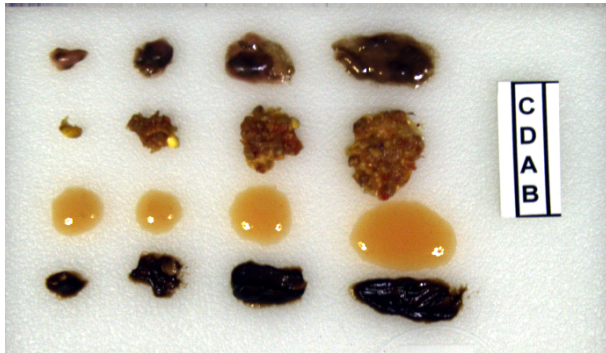
Figure 6. LED junction temperature vs. time for six-ring LED with heat sink.



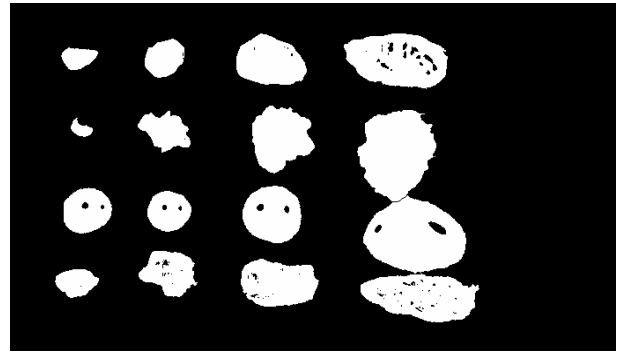
(a)



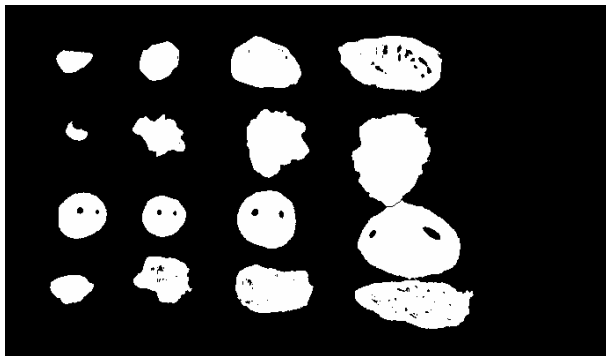
(d)



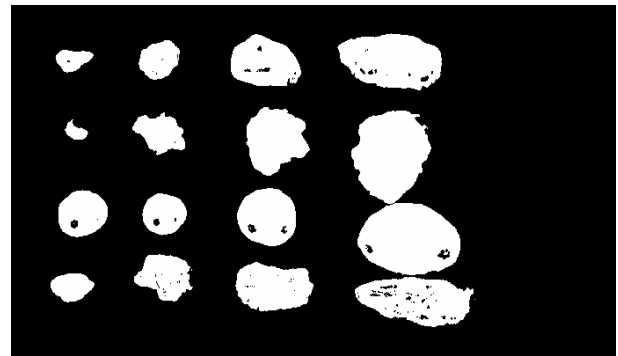
(b)



(e)



(c)



(f)

Figure 7. Color images (a) and (b), mask images (c) and (d), and predicted images (e) and (f) with tungsten-halogen and LED lighting, respectively. Contaminants are from top to bottom: ceca, ingesta, duodenum, and colon.

time variation. As can be seen, the output of the LED stabilized after about 25 min when the temperature roughly equilibrated. The temperature ripple occurring after that time was caused by the room air-conditioning cycling on and off. Thus, the LEDs were suitable for use after about 30 min or when the junction temperature stabilized at about 43°C.

However, even after the warm-up time during the preliminary experiments, at certain camera exposure settings, illumination variance across a given image was observed. It was determined that this spatial ripple was caused by the LED driver. Although the driver was recommended by the LED manufacturer and was marketed as a DC driver, the signal conditioning was not sufficient to remove all alternating current ripple that was noted on the images. Therefore, these drivers were discarded in favor of a true DC driver that provided ripple-free output. Thus, for subsequent measurements, the Monster Lights with their 24V DC driven drivers were used. Similar experiments were carried out with the QTH lamps and results indicated that the

QTH lamps stabilized much faster and with much less variations, and no ripple due to a true DC source. Thus, it was determined that the QTH lamps needed to equilibrate for 10 min prior to measurement.

#### FECAL ACCURACIES

Sixteen separate fecal samples were imaged in two orientations with each set of lights (figs. 7a-7b). Next, using HyperVisual software (Photon Industries, Stennis Space Center, Miss.), the fecal images were first calibrated to wavelength values and then to percent reflectance with the Spectralon and dark current measurements. Prior to using the calibration measurements, the duplicate Spectralon and dark current images were averaged to reduce random noise with ENVI (Research Systems, Inc., Boulder, Colo.). The calibration measurements taken immediately prior to a given fecal measurement were used to calibrate that fecal measurement. To match the output of the trim filters used in the multispectral fecal detection system, the calibrated image

files were then spectrally resampled with a 10-nm full width half max Gaussian filter function. Since the fecal material was imaged on a white Teflon cutting board and false positives are irrelevant on such a surface, any pixels associated with the cutting board (or the black marker and lettering used to identify the contaminants) were removed prior to analyzing the data. To remove the “white” cutting board, any pixels with reflectance values greater than 30% at 446 nm were masked. The black marker and lettering were removed with a maximum threshold of 0.85 for a ratio of a 500-nm image divided by a 600-nm image. Furthermore, the obvious specular reflectance, seen in some of the samples (figs. 7a and 7b), was also removed from the analysis with the mask described above as shown in figures 7c and 7d. Next, the background mask was used to create a classification ground-truth image for the duodenum, ceca, colon, and ingesta pixels. Primarily due to the variations in the specular reflectance between the two lighting systems, this process resulted in differences in the numbers of ground-truth pixels for a given fecal spot illuminated by the two lighting systems.

Thus, for meaningful results, comparisons between the lighting systems were done on a percent basis. Finally, an image ratio with a global threshold was used to predict contaminants. Based on previous research (Park et al., 2002, 2004), a reflectance image centered at 565 nm divided by a reflectance image centered at 517 nm with a global threshold of 1.05 was used. Typical results are shown in figures 7e and 7f for the QTH and LED lights, respectively.

Table 1 shows the accuracy of fecal detection for the two lighting systems. With both lighting systems, duodenum and ingesta samples were both detected at a very high accuracy of 99.99% and 100%, respectively. The ceca accuracies were just slightly less, as were most of the colon samples. However, the two images of the first colon sample, which had accuracies in the mid 70’s, and the last colon sample were noticeably lower. The regions of the colon samples that were not detected contained red-pigmented material which appeared to be blood mixed in the feces. Table 2 shows the total number of ground-truth pixels for each contaminant for each lighting system along with the overall accuracies and

**Table 1. Accuracies and means for poultry contaminants detected with a hyperspectral imaging system with LED or quartz-tungsten halogen (QTH) lighting.<sup>[a]</sup>**

Name	LED Duo	LED Ceca	LED Colon	LED Inges.	LED Total	QTH Duo	QTH Ceca	QTH Colon	QTH Inges.	QTH Total
1A	99.92	99.40	73.41	100.00	94.59	99.92	99.94	75.66	100.00	95.94
1B	99.98	99.87	73.38	100.00	94.82	99.99	99.96	77.22	100.00	96.33
2A	99.99	100.00	99.98	100.00	100.00	100.00	99.99	99.58	100.00	99.94
2B	99.99	100.00	99.98	100.00	100.00	100.00	99.97	99.96	100.00	99.98
3A	99.99	99.99	100.00	100.00	99.99	100.00	99.99	99.95	100.00	99.99
3B	100.00	99.99	99.99	100.00	100.00	99.99	99.93	100.00	100.00	99.98
4A	99.99	99.97	99.93	100.00	99.97	99.99	99.65	99.97	100.00	99.91
4B	100.00	99.99	100.00	100.00	100.00	100.00	99.94	99.89	100.00	99.96
5A	99.92	99.99	99.85	99.97	99.93	99.95	99.76	99.89	100.00	99.89
5B	99.94	99.95	99.92	100.00	99.95	99.96	99.81	99.92	100.00	99.92
6A	100.00	99.99	99.79	100.00	99.94	100.00	99.69	99.81	100.00	99.88
6B	100.00	99.99	99.92	100.00	99.97	99.99	99.65	99.93	100.00	99.91
7A	100.00	100.00	99.99	100.00	100.00	100.00	99.95	99.88	100.00	99.96
7B	100.00	99.99	99.98	100.00	99.99	99.98	99.97	99.95	100.00	99.97
8A	100.00	99.92	99.94	100.00	99.97	100.00	99.72	99.98	100.00	99.93
8B	99.99	100.00	99.96	100.00	99.99	100.00	99.82	100.00	100.00	99.96
9A	99.99	99.98	99.91	100.00	99.97	100.00	99.96	99.96	100.00	99.98
9B	100.00	100.00	99.98	100.00	99.99	100.00	99.95	99.97	100.00	99.98
10A	100.00	100.00	99.97	100.00	99.99	99.99	99.93	99.98	100.00	99.97
10B	100.00	99.99	100.00	100.00	100.00	99.99	99.92	100.00	100.00	99.98
11A	100.00	100.00	99.96	100.00	99.99	100.00	99.96	99.92	100.00	99.98
11B	99.99	100.00	100.00	100.00	100.00	99.98	100.00	99.90	100.00	99.98
12A	100.00	100.00	100.00	100.00	100.00	100.00	99.96	100.00	100.00	99.99
12B	99.99	100.00	99.96	100.00	99.99	100.00	99.96	99.96	100.00	99.98
13A	99.98	100.00	99.93	100.00	99.98	100.00	99.83	99.93	100.00	99.95
13B	100.00	100.00	99.89	100.00	99.98	100.00	99.78	99.95	100.00	99.94
14A	100.00	99.98	99.94	100.00	99.98	100.00	99.74	99.98	100.00	99.92
14B	99.99	99.99	99.99	100.00	99.99	99.98	99.55	99.99	100.00	99.86
15A	99.97	99.97	99.99	100.00	99.98	99.99	100.00	99.96	100.00	99.98
15B	100.00	99.98	100.00	100.00	100.00	99.99	99.98	99.99	100.00	99.99
16A	100.00	100.00	98.23	100.00	99.61	100.00	99.97	98.35	100.00	99.61
16B	99.99	100.00	98.25	100.00	99.62	100.00	99.97	98.34	100.00	99.62
Mean	99.99	99.97	98.19	100.00	99.63	99.99	99.88	98.37	100.00	99.69

<sup>[a]</sup> A and B refer to the two orientations for each sample.

the differences. Overall mean pixel counts for the fecal samples were 39,685 and 44,625 for the QTH and LED lights, respectively. The LED images had a significantly ( $p < 0.05$ ) higher number of ground-truth pixels than the QTH images. This was caused by a greater number of specular reflectance pixels masked out in the QTH images. There was little difference between the accuracies of the two systems. The hypothesis that the LED lighting performed better than the QTH lighting for use in detecting contaminants was rejected ( $p < 0.05$ ) with a paired t-test. Examining the data showed that the hypothesis was rejected primarily because of the first colon sample which had large differences of -1.35 and -1.5% while the next closest difference was only 0.13%. Thus, the LED lighting hypothesis might have been rejected because of problems with the detection algorithm itself.

## CONCLUSIONS

Both LED and quartz tungsten halogen lighting were useful for illumination in a hyperspectral imaging system for fecal detection. Detection accuracies were generally better than 99% for all contaminant types with either lighting system although there was one colon sample that had a rather low accuracy, most likely due to blood in the sample. Results indicated that there was no significant difference in detecting fecal contaminants with the fecal detection algorithm that used the ratio of images centered at 565 and 517 nm with either lighting system. Other advantages of LED illumination are higher efficiencies, less heat, and much longer lamp life (>10,000 h). Disadvantages are light intensity can vary with junction temperature and lower light intensities as compared to tungsten-halogen lights. Thus, given that there are no differences in detection results with the added benefits just mentioned, LED can be considered a better source of illumination for multispectral fecal detection than quartz tungsten halogen lamps, provided one can maintain a

**Table 2. Total number of ground-truth pixels and overall accuracy for a hyperspectral imaging system with LED or quartz-tungsten halogen (QTH) lights.<sup>[a]</sup>**

Number	Sample	QTH (# pixels)	LED (# pixels)	DIFF (# pixels)	LED Accuracy (%)	QTH Accuracy (%)	DIFF Accuracy (%)
1	1A	32101	27902	4199	94.59	95.94	-1.35
2	1B	32431	29090	3341	94.82	96.33	-1.51
3	2A	37144	42749	-5605	100.00	99.94	0.06
4	2B	37133	42531	-5398	100.00	99.98	0.01
5	3A	41520	42620	-1100	99.99	99.99	0.01
6	3B	41974	42777	-803	100.00	99.98	0.02
7	4A	38942	43614	-4672	99.97	99.91	0.06
8	4B	39532	43999	-4467	100.00	99.96	0.04
9	5A	43358	50621	-7263	99.93	99.89	0.04
10	5B	43916	51317	-7401	99.95	99.92	0.04
11	6A	39785	44133	-4348	99.94	99.88	0.06
12	6B	40592	43245	-2653	99.97	99.91	0.07
13	7A	38372	44895	-6523	100.00	99.96	0.04
14	7B	38817	45341	-6524	99.99	99.97	0.02
15	8A	40449	52663	-12214	99.97	99.93	0.05
16	8B	40730	53144	-12414	99.99	99.96	0.03
17	9A	42879	47066	-4187	99.97	99.98	-0.01
18	9B	43613	47255	-3642	99.99	99.98	0.01
19	10A	47613	51552	-3939	99.99	99.97	0.02
20	10B	48061	51233	-3172	100.00	99.98	0.02
21	11A	30486	31293	-807	99.99	99.98	0.01
22	11B	30846	31590	-744	100.00	99.98	0.02
23	12A	37684	43160	-5476	100.00	99.99	0.01
24	12B	38328	42935	-4607	99.99	99.98	0.01
25	13A	36686	44072	-7386	99.98	99.95	0.03
26	13B	36990	43734	-6744	99.98	99.94	0.03
27	14A	43972	52444	-8472	99.98	99.92	0.06
28	14B	44969	52071	-7102	99.99	99.86	0.13
29	15A	39713	51335	-11622	99.98	99.98	0.00
30	15B	40399	50958	-10559	100.00	99.99	0.01
31	16A	40200	43661	-3461	99.61	99.61	0.00
32	16B	40675	42998	-2323	99.62	99.62	0.01
Mean		39685	44625	-4940.3	99.63	99.69	-0.06
Std. dev.		4251.1	6772.7	3888.9	1.30	0.94	0.36

<sup>[a]</sup> A and B refer to the two orientations for each sample.

relatively constant junction temperature for the LEDs. Similar results should be expected with a high-speed hyperspectral imaging systems, but must be further evaluated.

## REFERENCES

- Heitschmidt, G. W., K. C. Lawrence, W. R. Windham, B. Park, and D. P. Smith. 2004. Improved imaging system for fecal detection. *Proc. SPIE* 5587: 112-120.
- Lawrence, K. C., B. Park, W. R. Windham, and C. Mao. 2003a. Calibration of a pushbroom hyperspectral imaging system for agricultural inspection. *Transactions of the ASAE* 46(2): 513-521.
- Lawrence, K.C., W. R. Windham, B. Park, and R. J. Buhr. 2003b. Hyperspectral imaging system for identification of fecal and ingesta contamination on poultry carcasses. *J. Near-Infrared Spectroscopy* 11(4): 269-281.
- Lawrence, K.C., W.R. Windham, B. Park, G.W. Heitschmidt, D. P. Smith, and P. Feldner. 2006. Partial least squares regression of hyperspectral images for contaminant detection on poultry carcasses. *J. Near-Infrared Spectroscopy* 14(4): 223-230.
- Mueller-Mach, R., G. O. Mueller, M. R. Krames, and T. Trottier. 2002. High-power phosphor-converted light emitting diodes based on III-nitrides. *IEEE J. Select. Topics Quantum Electron.* 8(2): 339-345.
- Muthu, S., F. J. P. Schurmans, and M. D. Pashley. 2002. Red, green and blue LEDs for white light illumination. *IEEE J. Select. Topics Quantum Electron.* 8(2): 333-338.
- Park, B., K. C. Lawrence, W. R. Windham, and R. J. Buhr. 2002. Hyperspectral imaging for detecting fecal and ingesta contaminants on poultry carcasses. *Transactions of the ASAE* 45(6): 2017-2026.
- Park, B., K. C. Lawrence, W. R. Windham, and D. P. Smith. 2004. Multispectral imaging system for fecal and ingesta detection on poultry carcasses. *J. Food Proc. Engr.* 27(5): 311-327.
- Steigerwald, D. A., J. C. Bhat, D. Collins, R. M. Fletcher, M. O. Holcomb, M. J. Ludowise, P. S. Martin, and S. L. Rudaz. 2002. Illumination with solid state lighting technology. *IEEE J. Select. Topics Quantum Electron.* 8(2): 310-320.
- Windham, W. R., K. C. Lawrence, B. Park, L. A. Martinez, M. A. Lanoue, D. A. Smith, J. Heitschmidt, and G. H. Poole. 2003a. Method and system for contaminant detection during food processing. U.S. Patent No. 6,587,575.
- Windham, W. R., K. C. Lawrence, B. Park, and R. J. Buhr. 2003b. Visible/NIR spectroscopy for characterizing fecal contamination of chicken carcasses. *Transactions of the ASAE* 46(3): 747-751.